

# 1 Analysis of the Jahn-Teller effect in Coronene and Corannulene ions 2 and its effect in EPR spectroscopy

3  
4 Francesco Tampieri<sup>a,†</sup>, Antonio Barbon<sup>a,\*</sup> and Matteo Tommasini<sup>b,\*</sup>

5  
6 <sup>a</sup> Dipartimento di Scienze Chimiche, Università degli Studi di Padova, Via Marzolo 1, 35131 – Padova,  
7 Italy.

8 <sup>b</sup> Dipartimento di Chimica, Materiali e Ingegneria Chimica, Politecnico di Milano, Piazza Leonardo da  
9 Vinci 32 – 20133 Milano, Italy.

10 <sup>†</sup> Present Address: Biomaterials, Biomechanics and Tissue Engineering Group, Department of Materials  
11 Science and Engineering, Technical University of Catalonia (UPC), c. Eduard Maristany 16, 08019 Bar-  
12 celona, Spain.

13 \* Corresponding authors: [antonio.barbon@unipd.it](mailto:antonio.barbon@unipd.it), [matteo.tommasini@polimi.it](mailto:matteo.tommasini@polimi.it)

## 14 15 **Abstract**

16 Coronene and corannulene are popular structures that have provided the basis for the investiga-  
17 tion of extended carbon-based structures, like graphene, fullerene and their derivatives. Here we  
18 address the Jahn-Teller (JT) effects in electron paramagnetic resonance (EPR) spectroscopy of  
19 such molecules in ionic form. By density functional theory (DFT) and a Monte Carlo based  
20 sampling of the potential energy surface, we obtain three and five symmetry-related JT equiva-  
21 lent conformers in coronene and in corannulene ions, respectively. The structure and the inter-  
22 conversion between the JT distorted forms are discussed for their implication in EPR spectros-  
23 copy. The calculation of the  $g$ -tensor by DFT methods has also been benchmarked to serve as  
24 methodological approach for the investigation of more extended graphene molecules.

25  
26 **Keywords.** Coronene, corannulene, electron paramagnetic resonance, density functional  
27 theory, Jahn-Teller,  $g$ -tensor

## 28 29 **Introduction**

30 Coronene and corannulene are representative members of the family of polycyclic aro-  
31 matic hydrocarbons (PAHs) compounds. PAHs have attracted (and still attract) consid-  
32 erable scientific and technological interest for a number of different reasons. They pro-  
33 vide an ideal ground for the developments of  $\pi$ -bonding theories [1,2] and the assess-  
34 ment of aromaticity in higher PAHs, such as coronene and corannulene, is still matter of  
35 research [3,4]. PAHs bear astrophysical relevance since they are thought to be present in

36 interstellar media as charged species [5–10]. The occurrence of PAHs as combustion  
37 products and their toxicity raise health and environmental concerns [11].  
38 Due to extended  $\pi$ -conjugation, the optical and electronic properties of PAHs are ap-  
39 pealing for materials science [12]. For instance, corannulene behaves as a good electron  
40 acceptor, even in solid-state films [13]. Furthermore, the inherent propensity of PAHs to  
41  $\pi$ -stacking (including the case of non-planar corannulene, see for instance the work of  
42 Yamada et al. [14]), may drive the self-assembly of structures characterized by useful  
43 transport properties for molecular electronics [15–17] and photonics [18].  
44 Another important aspect of PAHs is that they constitute molecular models of graphene,  
45 a material with unique properties [19] that has been investigated through several tech-  
46 niques, including electron paramagnetic resonance (EPR) [20]. An effort is put today on  
47 the study of real graphene-like systems, with characteristics that lead them far from the  
48 ideality of the graphene lattice, such as limited dimensions (*i.e.*,  $\pi$ -conjugation confine-  
49 ment), presence of defects or functional groups, or bending of the planar structure  
50 [21,22]. The joint effect of these peculiarities may impart to these systems different  
51 properties that can be used to tune the materials toward specific applications. Several  
52 theoretical methods have been considered to include these effects (see the work of  
53 Kheirabadi et al. [23] and references therein). The joint use of density functional theory  
54 (DFT) methods and molecular dynamics has shown to be particularly useful for model-  
55 ing the properties of these systems [24–26]. Furthermore, thanks to advances in compu-  
56 tational chemistry software and computers, informative calculations can be carried out  
57 on a relatively wide range of molecular sizes, thus making the molecular approach ap-  
58 pealing to graphene (*i.e.*, the bottom-up approach) [27].  
59 In the study of molecular graphene a relatively small number of papers have been pub-  
60 lished which include EPR investigation of these materials [20,28], as compared to other  
61 experimentally available techniques. EPR spectroscopy allows studying paramagnetic  
62 centers, also in the presence of ferromagnetic (or antiferromagnetic) exchange interac-  
63 tions. The high selectivity of EPR enables determining the presence of different types of  
64 contributions in the spectra of graphene-like samples [20,28–31]. In different kinds of  
65 graphite-like materials the typically accessible experimental EPR parameter ( $g$ -tensor)  
66 show a variability of values that has not been yet associated to descriptors of the materi-  
67 al structure, such as the presence of edge states, defects, or bending of the graphene  
68 flakes [29,32,33]. We believe that this gap is one of the possible reasons that prevented  
69 a wider use of EPR in the characterization of graphene-like systems.

70 In this work, we begin filling this gap, by starting a study of the effects on EPR spectra  
71 of what we could define as *perturbations* to the ideal structure of graphene. Unfortu-  
72 nately, the variety of perturbations can be rather wide (*e.g.*, different edge topology,  
73 influence of heteroatoms, strain of the honeycomb structure/topological defects, *etc.*  
74 [34–36]). For this reason, we decided to focus on the calculation of the  $g$ -tensor of sim-  
75 ple molecules with extended  $\pi$ -conjugation, subject to Jahn-Teller (JT) distortion, con-  
76 sidering the effects of curvature, which are caused by a local disruption of the honey-  
77 comb motif (*i.e.*, the topological defect caused by the substitution of a hexagonal ring  
78 with a pentagonal ring). Due to the availability of experimental and theoretical data to  
79 compare with, the chosen molecules are coronene (planar) and corannulene (bent).  
80 Coronene is representative of an H-terminated nano-graphene with lateral dimension of  
81 approximately 1 nm. This highly symmetric molecule ( $D_{6h}$  point group) possesses de-  
82 generate HOMO and LUMO levels, thus undergoing JT distortion upon removal or ad-  
83 dition of an odd number of electrons. This issue has been assessed in the 60’s for a se-  
84 ries of highly symmetric aromatic ions, like benzene and simple polyaromatics, includ-  
85 ing coronene. Results from Hückel calculation and EPR measurements of hyperfine  
86 interactions and linewidths convey to state that such a distortion is present in the highly  
87 symmetric molecules, and that polar solvents play a role on this [37]. Forty years later  
88 more accurate DFT calculations by Kato et al. showed that the inclusion of JT distortion  
89 affords excellent agreement with experiment in the vibrational frequencies of coronene  
90 [38]. However, even if particularly careful and accurate, this study still shows the pres-  
91 ence of a slight instability in the potential energy surface with associated imaginary  
92 wavenumber modes. The authors, in another work, calculated the vibrational spectrum  
93 for corannulene, showing also in that case a removing of the degeneracy of the orbital  
94 by a distortion of the molecule [39]. JT effects, in a work by Galué et al., has been  
95 shown to be more important for corannulene with respect to coronene [40].  
96 Experimental evidence for the anions was given by the X-ray diffraction analysis con-  
97 ducted by Filatov et al. [41]. A further study by Andjelković et al. calculated vibrational  
98 frequencies and determined a very low energy barrier between the symmetry-related JT  
99 distorted forms [26].  
100 At first, our present investigation aims at providing geometries with fully stable energy  
101 minima of the JT distorted structures of corannulene and coronene ions and to obtain  
102 vibrational frequencies to be compared to previously determined experimental geome-  
103 tries and experimental and calculated vibrational frequencies [38]. This will serve for

104 further investigation on the magnetic properties of the molecule, in particular we will  
105 consider the calculation of the  $g$ -tensor, related to experimental observables, and discuss  
106 the effect of the JT distortion of both molecules in the anionic and in the cationic forms.  
107 The DFT results are critically discussed and compared to available experimental data.

108

## 109 **Methods**

110 The neutral ground states of highly symmetric coronene ( $D_{6h}$ ) and corannulene ( $C_{5v}$ )  
111 have doubly degenerate HOMOs and LUMOs. Hence, the addition (removal) of one  
112 electron to form an ion causes the partial filling of the doubly degenerate LUMOs  
113 (HOMOs), which is the classical situation leading to JT distortion. This means that the  
114 molecule is prone to change its structure (relax) and reduce its point group symmetry.  
115 With this picture in mind, we set a Monte Carlo inspired exploration of the JT structures  
116 of the anions and cations of coronene and corannulene in the following way. We began  
117 with the reference optimized structures of the neutral ground state ( $X_0$ ), and we added a  
118 small random perturbation ( $\delta X$ ) whose immediate effect is to slightly lift the degeneracy  
119 of the HOMOs and LUMOs, in a way that depends on the particular realization of  $\delta X$ .  
120 The perturbation added to the position of each atom was defined as a random vector  $v$   
121 picked up from a uniform distribution of points on a sphere of radius 0.001 Å. The re-  
122 quired random vectors  $v$  were evaluated with a convenient approach devised by Marsa-  
123 glia [42]. The structure  $X_0 + \delta X$  was then taken as the initial structure for tight geometry  
124 optimization of the anion/cation species. By repeating the procedure for different ran-  
125 dom choices of  $\delta X$  it is possible to effectively explore the potential energy surface of the  
126 JT potential, easily recovering the different equivalent minima. Tight optimization and  
127 tight SCF convergence were crucial to get final structures of the expected symmetry  
128 [43], with no imaginary vibrational frequencies. About 20 Monte Carlo runs were  
129 enough to recover all the expected deformed structures (based on the initial molecular  
130 symmetry, see further) for each charged species.

131 All calculations have been carried out on isolated molecules based on DFT, by consid-  
132 ering the widely adopted B3LYP hybrid functional, which is known to provide reliable  
133 equilibrium molecular structures (also adopted in the work by Kato et al. [38]). There-  
134 fore, we used Gaussian09 with the B3LYP/6-311G(d,p) method. We have then calculat-  
135 ed the vibrational frequency for all the optimized structures to assess that they were ac-  
136 tual minima (with no negative eigenvalues of the Hessian). These optimized structures  
137 were used for the DFT calculations of the  $g$ -tensors. We used the ORCA quantum

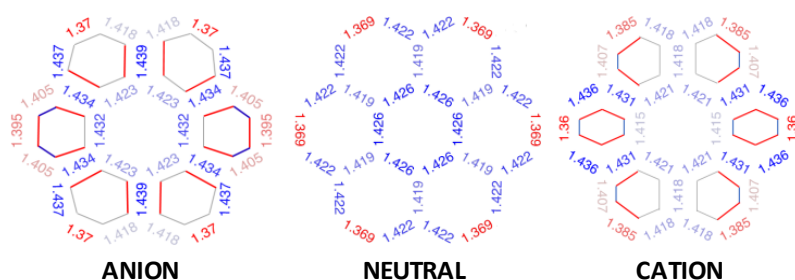
138 chemistry code (version 4.2.1) [44] testing several basis sets within the GIAO approach  
139 [45] and the RI-JK approximation (def2/JK keyword).

140

### 141 **Calculation of the vibrational frequencies**

142 The equilibrium bond length have been obtained by DFT for the neutral coronene in  $D_{6h}$   
143 symmetry and have been compared with those computed by Kato [38], and the experi-  
144 mental values [46]. The result of this comparison is reported in Table SII, and shows a  
145 good agreement both considering previous calculations, and experimental values.  
146 Therefore, following the procedure described in the Methods section, we have obtained  
147 for coronene the three symmetry-related stable equilibrium geometries of both ions (no  
148 imaginary frequencies were observed in such JT distorted structures, see Figure 1). As  
149 expected, the three equivalent JT forms of both ions display lower symmetry than the  
150 neutral forms ( $D_{2h}$  vs.  $D_{6h}$ ) and are related one another by a  $C_3$  rotation around the axis  
151 orthogonal to the molecular plane.

152



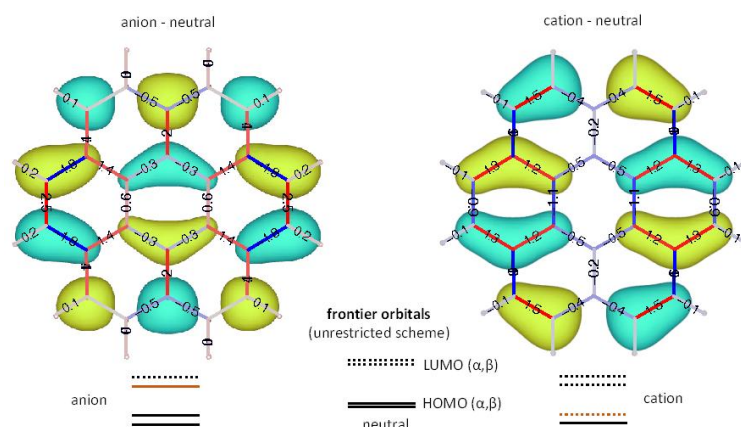
154

155 **Figure 1.** Bond lengths of one JT distorted equilibrium structure (the other two are symmetry-related  
156 obtained by  $C_3$  rotation) of coronene anion (left) and cation (right). The sketched hexagons emphasize the  
157 distortion of the rings from the neutral form (blue: shortening, red: lengthening, grey: almost unaffected).  
158 The neutral form is shown for reference (centre).

159

160 The pattern of equilibrium bond length obtained for the JT distorted coronene ions can  
161 be justified by considering the spatial distribution of the frontier orbitals (Figure 2). For  
162 instance, the bonds of the anion, which elongate compared to their length in the neutral  
163 structure, are all associated to positions where the singularly occupied molecular orbital  
164 (SOMO) displays a nodal plane approximately bisecting the bond. In other words, the  
165 SOMO introduces antibonding character in these positions, which causes bond elonga-  
166 tion passing from the neutral to the anionic form. Conversely, the bonds where the

166



167

168 **Figure 2.** JT analysis of coronene anion (left) and cation (right): The variation of the bond length with  
 169 respect to the neutral form (blue bonds correspond to a shortening, and red bonds to an elongation) is  
 170 shown. Selected frontier spin-orbitals are shown overlapped with each structure to justify the observed  
 171 structure relaxation patterns (see text and ESI for additional details). The JT distorted structures of the  
 172 coronene anion and cation both belong to the  $D_{2h}$  point group symmetry. The electronic wavefunction of  
 173 the anion is  $2-B_{2g}$  and that of the cation is  $2-A_u$ .

174

175 SOMO displays a bonding character are all becoming shorter in the anion compared to  
 176 the neutral form.

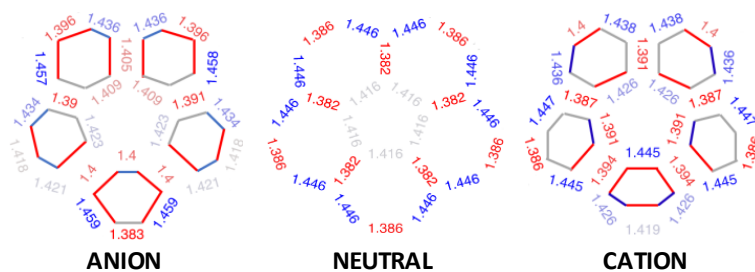
177 In the case of coronene cation, to rationalize the obtained structure relaxation displayed  
 178 in Figure 2, one should consider the orbital from which the electron was formally  
 179 removed (*i.e.* the  $HOMO\beta$ ). Upon removing of the electron, the orbital becomes a SOMO,  
 180 and the reduction of density affects the bond lengths: bonds where SOMO is bonding  
 181 elongates in the cation, because of the removal of the electronic bonding charge. Con-  
 182 versely, the bonds having antibonding contribution from the SOMO become shorter,  
 183 because of the reduction of this antibonding contribution upon ionization.

184 Considering the values of the bond lengths changes between the ionic and neutral form,  
 185 we see from Figure 2 that the JT distortion affects principally the radial and edge CC  
 186 bonds of coronene. Due to the placement of the elongating bonds (all aligned along the  
 187 vertical axis in Figure 2) in coronene anion the JT distortion causes a net stretching of  
 188 the molecule along the vertical axis, which leads to the reduction of symmetry from  $D_{6h}$   
 189 to  $D_{2h}$ . Since there are three equivalent axes along which the stretching of coronene may  
 190 occur, we count three equivalent JT distorted forms in coronene anion as anticipated  
 191 earlier.

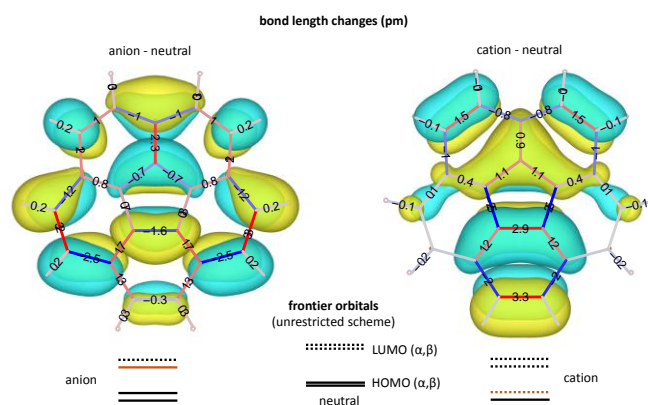
192 In the case of coronene cation, compared to the neutral  $D_{6h}$  structure, the molecule un-  
 193 dergoes a contraction along the vertical axis of Figure 2, for reasons similar (but oppo-  
 194 site) to the case of the anion, and a stretching along the horizontal axis.

195 We have carried out the same kind of theoretical analysis of the JT distortion also for  
 196 corannulene, in both anionic and cationic state. Figure 3 shows the equilibrium structure  
 197 of one out of the five equivalent JT distorted equilibrium structures of the ionic forms of  
 198 corannulene (both belonging to  $C_s$  point group). These are compared with the equilibri-  
 199 um structure of neutral corannulene (belonging to the  $C_{5v}$  point group). The geometry  
 200 relaxation driven by the JT distortion can be better inspected in Figure 4, where it is  
 201 compared with the relevant frontier orbital. This orbital is the one that differs between  
 202 the charged and the neutral state. Similar to the previous case of coronene, all CC bond  
 203 changes can be rationalized by the inspection of the nodal pattern of the frontier orbitals  
 204 of interest. Notably, compared with the equilibrium structure of neutral corannulene, the  
 205 CC bonds of the anion become shorter where the orbital of the added electron display a  
 206 bonding character. This is the opposite in the case of the cation: here CC bonds becom-  
 207 ing shorter where the orbital of the removed electron has antibonding character (*i.e.* it  
 208 displays a nodal plane bisecting the bond).  
 209 We note that the CC bond variations with respect to the neutral form are slightly higher  
 210 in corannulene than in coronene (compare Figure 4 with Figure 2).

211  
 212



213 **Figure 3.** Bond lengths of JT distorted equilibrium structure (the other four are symmetry-related ob-  
 214 tained by  $C_5$  rotations) for corannulene anion (left) and cation (right): The hexagon emphasize the distort-  
 215 tion of the rings from the neutral form (blue: shortening, red: lengthening, grey: almost unaffected). The  
 216 neutral form is shown for reference (centre).  
 217  
 218



219

220 **Figure 4.** JT analysis of corannulene anion (left) and cation (right): The variation of the bond length with  
 221 respect to the neutral form (blue bonds correspond to a shortening, and red bonds to an elongation) is  
 222 shown. Selected frontier spin-orbitals are shown overlapped with each structure to justify the observed  
 223 structure relaxation patterns (see text and SI for additional details). The JT distorted structures of the  
 224 corannulene anion and cation both belongs to the  $C_s$  point group symmetry and their electronic wavefunc-  
 225 tion is  $2-A'$ .

226

227 The vibrational structure and IR transitions of the cations of coronene and corannulene  
 228 have been carefully addressed in the past [26,40,47,48], driven by the interest in PAHs  
 229 as sources of IR emission bands observed in the astrophysical context [49]. Three mid-  
 230 IR bands of the coronene cation have been observed in matrix-isolated experiments  
 231 [50]. The results from previous DFT calculations [47] and those presented in this work  
 232 correlate very well with such experimental findings, which supports the conclusion that  
 233 the coronene cation possess just one JT distorted form (Table 1 and Table SI1). The  
 234 same conclusion was reached by multideterminantal-DFT and intrinsic distortion path  
 235 methods [26].

236

237 **Table 1.** The observed IR transitions of the cation of coronene, compared with present results from DFT  
 238 calculations. The representation of the normal modes taken from B3LYP/cc-pVTZ results is also provid-  
 239 ed (this is very close to that of B3LYP/6-311G(d,p) normal modes) (see ESI for the representation of the  
 240 associated nuclear displacements).

Expt. [50]	Matrix	B3LYP/cc-pVTZ ( $\text{cm}^{-1}$ , km/mol)	B3LYP/6-311G(d,p) ( $\text{cm}^{-1}$ , km/mol)	irrep	mode description
875		903 (145)	894 (160)	$B_{3u}$	(a)
1379		1392 (289)	1393 (302)	$B_{1u}$	(b)
1579		1605 (413)	1605 (426)	$B_{1u}$	(c)

241 (a) collective in-phase CH out-of-plane bending

242 (b) D-mode displacement of rings (A, B) out-of-phase vs. rings (F, G)

243 (c) G-mode displacement of rings (F, G) out-of-phase vs. rings (A, B)

244 Quite remarkably, differently from the coronene cation, the corannulene cation was re-  
 245 ported to possess two inequivalent JT distorted forms [40]. Our present analysis, based  
 246 on a Monte Carlo sampling of the PES of the corannulene cation, followed by tight full  
 247 geometry optimization (see Methods), discards such possibility: no JT distorted stable  
 248 minimum other than that reported in Figure 3 was found. Moreover, we carefully  
 249 checked the JT distorted state identified by the CC bond lengths of the inner pentagon  
 250 given by 1.384 Å, 1.440 Å, and 1.408 Å (B3LYP/6-311G(d,p) calculation, table II of  
 251 the paper by Galué et al. [40]). **By re-computing such structure with tight convergence**  
 252 **thresholds, we actually found** a first-order saddle point with imaginary frequency of  
 253 about  $i30\text{ cm}^{-1}$ . This structure is interpreted as the transition state between equivalent JT  
 254 distorted minima, **similar to that found for  $\text{Cu}^{2+}$  impurities placed in cubic lattices with**  
 255 **fluorite structure [51].**

256

257 **Table 2.** The observed IR transitions of the cation of corannulene, compared with present results from  
 258 DFT calculations (see ESI for the representation of the associated nuclear displacements).

Expt. IRMPD [40]	B3LYP/cc-pVTZ ( $\text{cm}^{-1}$ , km/mol)	B3LYP/6-311G(d,p) ( $\text{cm}^{-1}$ , km/mol)	irrep	mode description
835	858 (32)	851 (4)	A''	(a <sub>1</sub> )
	860.9 (33)	857.7 (35)	A'	(a <sub>2</sub> )
	861.2 (18)	856.3 (50)	A''	(a <sub>3</sub> )
	899 (108)	891 (119)	A'	(a <sub>4</sub> )
1092	1033 (174)	1031 (175)	A'	(b)
1154	1097 (254)	1096 (227)	A'	(c <sub>1</sub> )
	1101 (357)	1101 (365)	A''	(c <sub>2</sub> )
	1105 (27)	1101 (63)	A'	(c <sub>3</sub> )
1222	1191 (79)	1190 (89)	A'	(d <sub>1</sub> )
	1209 (25)	1208 (24)	A'	(d <sub>2</sub> )
	1217 (75)	1215 (89)	A''	(d <sub>3</sub> )
1332	1292 (118)	1289 (118)	A'	(e <sub>1</sub> )
	1303 (178)	1300 (185)	A''	(e <sub>2</sub> )
1663	1572 (174)	1571 (174)	A''	(f <sub>1</sub> )
	1607 (179)	1606 (180)	A'	(f <sub>2</sub> )

259 (a<sub>1</sub>, a<sub>3</sub>, a<sub>4</sub>) collective CH out-of-plane bending

260 (a<sub>2</sub>) ring deformation, collective CH out-of-plane bending

261 (b) pentagonal ring deformation, CH bending, edge CC stretching

262 (c<sub>1</sub>, c<sub>2</sub>, c<sub>3</sub>) collective CC stretching, ring deformation, CH bending

263 (d<sub>1</sub>, d<sub>2</sub>, d<sub>3</sub>) collective ring deformation, CH bending

264 (e<sub>1</sub>, e<sub>2</sub>) ring stretching (reminiscent of graphene D mode)

265 ( $f_1, f_2$ ) ring stretching (reminiscent of graphene G mode)

266

267 It might be convenient to compare the calculated bond lengths of anions with experi-  
268 mental values from the crystals with alkaline counter ions [41] (X-ray diffraction data  
269 for the cations of coronene and corannulene could not be found in the literature). We  
270 refer the reader to ESI (Tables SI1 and SI2) for further comments.

271 In IR multiple-photon dissociation (IRMPD) experiments [40] the corannulene cation  
272 displays a larger number of IR transitions than the coronene cation, whose position is  
273 consistent with DFT calculations (Table 2). Compared with the coronene cation, the  
274 larger number of IR transitions observed in corannulene cation is due to the much less  
275 symmetric, non-planar structure (*i.e.*,  $C_s$  vs.  $D_{2h}$ ).

276

### 277 **Calculation of EPR parameters**

278 We calculated the  $g$ -tensors for the optimized geometries of the JT distorted ions, com-  
279 puted at the B3LYP/6-311G(d,p) level which in the previous section was deemed relia-  
280 ble in providing a good description of the vibrational structure of both coronene cation  
281 and corannulene cations. Therefore, we kept the same B3LYP functional and considered  
282 different basis sets to benchmark the sensitivity (Table 3) with respect to reference ex-  
283 perimental EPR data (Table 4). From a quick inspection, it is clear that the 6-  
284 311++G(d,p) basis set (including diffuse orbitals), is totally unsuited, also in anions,  
285 where the use of such functions is usually recommended [43]. All other basis sets pro-  
286 vide rather similar results, with differences of  $\pm 0.0001$  for the single principal values of  
287 the  $g$ -components. This accuracy of  $g$ -values is acceptable, as it is comparable with the  
288 accuracy of most EPR measurements. For the sake of completeness, we also checked  
289 the  $g$ -tensor calculations on the JT equilibrium geometries computed with the  
290 B3LYP/cc-pVTZ method; the results are reported in ESI (Table SI3) and display very  
291 minor differences (of the order of about  $\pm 10^{-4}$ ) with respect to the EPR calculations car-  
292 ried out on B3LYP/6-311G(d,p) equilibrium geometries. The Z-direction is taken per-  
293 pendicular to the  $\pi$ -system in coronene, or perpendicular to the central ring in corannu-  
294 lene. The isotropic values,  $g_{\text{iso}} = (g_1 + g_2 + g_z)/3$ , are between 2.0024 and 2.0025 for all  
295 the ions, but for the corannulene anion we find a slightly smaller value, in the range of  
296 2.0021-2.0023.

297

298

299 **Table 3.** Calculated energies ( $E$ ),  $g$ -tensor principal components (in-plane  $g_1$ ,  $g_2$ , and out-of-plane  $g_z$  –  
300 with respect to the internal hexagon/pentagon), isotropic value ( $g_{iso}$ ) and anisotropy parameter ( $\Delta g$ ) of the  
301  $g$ -tensor for the ions of coronene and corannulene.

Ion	Method	$E$ (Ha)	$g_z$	$g_1$	$g_2$	$g_{iso}$	$\Delta g$
coronene (+)	epr-ii	-921.15944491	2.0021108	2.0022486	2.0030216	2.0024603	0.0009108
	6-311G(d,p)	-921.26173606	2.0020811	2.0022619	2.0030656	2.0024695	0.0009845
	6-311++G(d,p)	-921.26774108	2.0008139	2.0405486	2.1553143	2.0655589	0.1545004
	cc-pVTZ	-921.35667918	2.0021122	2.0022356	2.0030705	2.0024728	0.0009583
	def2-tzvp	-921.37759747	2.0020988	2.0023057	2.0031360	2.0025135	0.0010372
	def2-tzvpp	-921.38261962	2.0020909	2.0022998	2.0031294	2.0025067	0.0010385
corannulene (+)	epr-ii	-767.46893487	2.0022817	2.0022527	2.0027789	2.0024378	0.0005262
	6-311G(d,p)	-767.55746144	2.0022656	2.0022557	2.0028119	2.0024444	0.0005562
	6-311++G(d,p)	-767.56311673	2.0069208	2.0054497	2.0103499	2.0075735	0.0049002
	cc-pVTZ	-767.63612739	2.0022759	2.0022679	2.0028286	2.0024575	0.0005607
	def2-tzvp	-767.65352199	2.0022790	2.0022639	2.0028518	2.0024649	0.0005879
	def2-tzvpp	-767.65763723	2.0022791	2.0022611	2.0028567	2.0024656	0.0005956
coronene (-)	epr-ii	-921.42403112	2.0017901	2.0023648	2.0031515	2.0024355	0.0013614
	6-311G(d,p)	-921.52804635	2.0017179	2.0024084	2.0032353	2.0024539	0.0015174
	6-311++G(d,p)	-921.54062213	1.9771523	2.0081684	2.0150916	2.0001374	0.0379393
	cc-pVTZ	-921.62384556	2.0017518	2.0025350	2.0032782	2.0025217	0.0015264
	def2-tzvp	-921.64694093	2.0017270	2.0022032	2.0032696	2.0023999	0.0015426
	def2-tzvpp	-921.65229166	2.0017294	2.0020745	2.0032696	2.0023578	0.0015402
corannulene (-)	epr-ii	-767.76064156	2.0013956	2.0024754	2.0029896	2.0022869	0.0015940
	6-311G(d,p)	-767.84982195	2.0011439	2.0025020	2.0030713	2.0022391	0.0019274
	6-311++G(d,p)	-767.86403122	1.9220340	1.9955501	2.0097528	1.9757790	0.0877188
	cc-pVTZ	-767.93034207	2.0011004	2.0025479	2.0031351	2.0022611	0.0020347
	def2-tzvp	-767.95062795	2.0010117	2.0024346	2.0030779	2.0021747	0.0020662
	def2-tzvpp	-767.95505687	2.0010529	2.0024079	2.0030854	2.0021821	0.0020325

302

303 Remarkably, the results from 6-311++G(d,p) method are not in line with these values,  
304 and well distant from those expected for organic molecules in general, mainly because  
305 of an overestimation of the paramagnetic contribution of the spin-orbit term.

306 We note that the anisotropy,  $\Delta g = \max(g_1, g_2, g_z) - \min(g_1, g_2, g_z)$ , of the cations is  
307 smaller than the anisotropy of the anions. Moreover, due to the JT symmetry lowering,  
308 in positively and negatively charged ions we obtained tensors with orthorhombic sym-  
309 metry.

310 We turn now to the comparison between the theoretical data of Table 3 and the experi-  
311 mental data of Table 4, relative to EPR measurements on fluid solutions. It is conven-  
312 nient to compare first the anions for which the experimental values are available for both  
313 coronene and corannulene.

314 **Table 4.** Experimental  $g$ -values for the ions of coronene and corannulene.

Ion	Solvent	$\langle g \rangle$	Ref.
Coronene (+)	H <sub>2</sub> SO <sub>4</sub>	2.00256	[52]
	hexafluoroisopropanol/Tl(III) trifluoroacetate	2.00260	[53]
	SbF <sub>5</sub> /SO <sub>2</sub> ClF/Tl(III) trifluoroacetate	2.00256	[54]
	/	2.0025	[55]
Corannulene (+)	<i>no experimental data available</i>		
Coronene (-)	DME/Na	2.003068	[56]
	THF/Na	2.0032	[57]
	/	2.0029	[55]
Corannulene (-)	propylene carbonate	2.0045	[58]
	THF/K, THF/Li	2.0027	[59]
	THF/Li	2.0025	[60]
	THF/Na, THF/K, DME/Alkyl ammonium ions	2.0027	[61]

315

316 The coronene anion displays a larger  $g_{\text{iso}}$  value than corannulene, and this experimental  
 317 trend is reproduced by the calculations. The calculation that deviates the most from the  
 318 experimental values is that on coronene anion, (0.0007), and the agreement is much  
 319 better for the corannulene anion. According to the theory by Stone, also extended to  
 320 degenerate states [37,62], one component ( $g_z$ ) is always close to  $g_e$ . However, P.W.  
 321 Atkins et al. [63] found that the solution of the Dirac equations bring more terms that  
 322 justify the deviations from  $g_e$ . Indeed, beside the relativistic contribution (-0.00014),  
 323 along the Z-direction we have both diamagnetic (0.00002–0.00004) and paramagnetic  
 324 spin-orbit contributions ( $g_{\text{PSO}}$ ) [44].

325 **The calculated terms are reported in the S.I. (TableSI4).** In all of the ions, one in-plane  
 326 component of the  $g_{\text{PSO}}$  contribution is large and positive. The Z-component is small for  
 327 the cations (and generally positive), but large and negative for the anions. Therefore, the  
 328 values in corannulene anion (in the range 2.0010–2.0013) are unexpectedly low. We  
 329 associate such low values to the presence of the pentagonal ring that induces a curvature  
 330 to the  $\pi$ -system. For instance, we note that low  $g$ -components are found in other related  
 331 carbon structures containing such characteristic moiety, like fullerene-type ions [64].  
 332 Finally, we notice that the  $g$ -value of the coronene cation is reproduced with a remarka-  
 333 ble accuracy, **while for the anions the relatively small mismatches are likely due to the**  
 334 **spin/orbit contributions, which have two relatively large components with opposite sign,**  
 335 **a situation that sometimes can induce instability.**

336 The JT distortion of the coronene and corannulene ions has been debated for a long  
337 time, and different approaches have been used. Because of the geometry optimization of  
338 JT distorted structures discussed above, in our models the JT distortion has been already  
339 considered for the interpretation of the EPR measurements. Notably, in a series of pa-  
340 pers focused on benzene and coronene anions in solution, the EPR spectra exhibited an  
341 unusual line broadening that was attributed to the JT effect [65–67]. However, it was  
342 unclear if the broadening was connected to the JT-induced modulation of the hyperfine  
343 interactions or to a modulation of the spin/orbit coupling (dynamic JT effect). At that  
344 time, the JT distortion was considered in detail for the calculation of the proton hyper-  
345 fine interactions, but the calculation carried out for the vibronic states showed that a  
346 symmetric state is plausible, as the distorted structures are slightly higher in energy, but,  
347 apparently, for EPR measurements in solution state, the solvent might play a major role  
348 in the stabilization of the JT forms [66].

349 A different conclusion was obtained by Sato et al. [68] after the analysis of the EPR  
350 spectra of the coronene ions that, differently from corannulene, exhibited 13 equally  
351 spaced lines down to 203 K that were taken as evidence of no JT distortion associated to  
352 the lowering of coronene symmetry. However, in ref. [68] the authors did not carry out  
353 a careful linewidth analysis, whereas this kind of analysis was the argument previously  
354 assumed in ref. [69] to invoke JT distortion. For corannulene, instead, the same authors  
355 concluded that the EPR data show unequivocally that the anion is distorted [69], be-  
356 cause at temperatures below 273 K the symmetry of the system is lowered and the EPR  
357 spectrum becomes more complex, with a large number of lines due to the presence of  
358 inequivalent protons. This was expected in the presence of a dynamic JT effect [70],  
359 with a relatively low interconversion barrier between the structures [26]. As a conse-  
360 quence, at high temperature, the fast interconversion between forms averages the hyper-  
361 fine interactions of all protons, so that they become equivalent [39]. Also, in a previous  
362 work by Baumgarten et al. [59], at 200 K the lowering of symmetry was not observed,  
363 and consequently the conclusion of the work was that the corannulene anion is highly  
364 symmetric.

365 An issue that is not apparently taken into account in the interpretation of the experi-  
366 mental EPR data is that neutral corannulene is a very flexible aromatic compound capa-  
367 ble of performing another conformational change: the bowl-to-bowl inversion, with an  
368 estimated energy barrier of  $10.2 \pm 0.2$  kcal/mol (i.e.,  $3570 \pm 70$  cm<sup>-1</sup>) [70]. If the energy  
369 barrier is almost the same also for the ions of corannulene, the bowl-to-bowl inversion

370 should also contribute mainly to the relaxation properties of the molecule (spectral lin-  
371 ewidth), but it should not affect the molecular magnetic parameters. Unfortunately, the  
372 corannulene cation is unstable and it is likely prone to polymerization [61], thus it has  
373 not been observed in solution so far.

374 Different types of calculation have been carried out especially for the anions of coran-  
375 nulene. The JT distortions in the mono anion of corannulene was found to drive a reduc-  
376 tion of the symmetry of the radical state from  $C_{5v}$  to  $C_s$  structures [39,70], in agreement  
377 with the results of our work (see Figure 4). In the work by Sato et al. [70] the energy  
378 difference  $\Delta E$  between the different JT forms and the TS was found to be about  $20 \text{ cm}^{-1}$ ,  
379 which also agrees with the value found in [26].

380 Regarding the calculation of the  $g$ -tensor, few papers deal with the estimation of this  
381 parameter in PAHs, and the first dealing with formally degenerate states was that by R.  
382 E. Moss and A. J. Perry [37], who extended Stone's theory to the case of degenerate  
383 states. They considered the case of benzene anion, and coronene as an extension of that  
384 case. The calculation was focused on the estimation of its trace, as the available experi-  
385 mental values (see Table 4) were obtained in fluid solution. They recognize the possible  
386 splitting of degenerate levels and  $g$ -factor deviations as due to coupling/combinations of  
387 JT inactive vibrations.

388 Here we claim that several JT distorted structures at the same energy are present, and  
389 they are separated by rather low energy barriers, therefore it is likely that these systems  
390 are subject to dynamical JT effects.

391 At the end of this discussion, we point out that other higher order spin-orbit terms for  
392 the  $g$ -tensor could be included in the model, but, so far, these calculations have been  
393 limited to small molecules [70].

394

## 395 **Conclusions**

396 By DFT calculations we investigated the impact of the Jahn-Teller distortion on the  
397 EPR spectroscopy of coronene and corannulene ions. By adopting tight convergence  
398 criteria, we have identified robust stable structures (no negative frequencies) of the neu-  
399 tral and JT distorted singly ionized forms of coronene and corannulene, revising and  
400 unifying the results available in the literature. A careful Monte-Carlo based optimization  
401 of the JT distorted equilibrium structures shows that a manifold of  $n$  symmetric replicas  
402 of *one single* distorted form is obtained for each ion of the two molecules, with  $n = 3$  for  
403 coronene and  $n = 5$  for corannulene. Based on the analysis of the frontier orbitals we

404 could justify the observed variations of the CC bond lengths while passing from the  
405 neutral form to the JT minima. The quite flat energy landscape in the vicinity of the  
406 stable minima and the low energy barrier between the JT conformers allows a relatively  
407 easy thermally-activated interconversion. *A posteriori*, this supports our choice to run  
408 DFT calculations with tight convergence criteria.

409 The results obtained for the IR transitions of the JT distorted cations of coronene and  
410 corannulene satisfactorily reproduce the experimentally available IRMPD data [40]. As  
411 for EPR spectroscopy, the calculated *g*-values quantitatively reproduce the experimental  
412 values to a satisfactory precision, with the exception of the coronene anion, which dis-  
413 plays a too low theoretical value. The computed *g*-tensor of the corannulene anion is of  
414 particular interest, since it shows the lowest principal value much smaller than  $g_e$ . This  
415 result is of particular interest for EPR spectroscopy of graphene-like systems, where low  
416 *g*-tensor components have been measured [29].

417 Finally, the JT distortion and the low activation energy for interconversion between  
418 conformers allows to understand the underneath cause of the unusual broadening of the  
419 lines of the EPR spectra discussed in the literature as function of temperature (see for  
420 instance ref.s [71] and [59]).

421

## 422 **Conflicts of interest**

423 There are no conflicts to declare.

424

## 425 **References**

- 426 [1] E. Clar, The Aromatic Sextet, in: *Mob. Source Emiss. Incl. Polycyclic Org. Species*, Springer  
427 Netherlands, Dordrecht, 1983: pp. 49–58. [https://doi.org/10.1007/978-94-009-7197-4\\_4](https://doi.org/10.1007/978-94-009-7197-4_4).
- 428 [2] G. Trinquier, J.-P. Malrieu, Predicting the Open-Shell Character of Polycyclic Hydrocarbons in  
429 Terms of Clar Sextets, *J. Phys. Chem. A.* 122 (2018) 1088–1103.  
430 <https://doi.org/10.1021/acs.jpca.7b11095>.
- 431 [3] M.A. Dobrowolski, A. Ciesielski, M.K. Cyrański, On the aromatic stabilization of corannulene and  
432 coronene, *Phys. Chem. Chem. Phys.* 13 (2011) 20557. <https://doi.org/10.1039/c1cp21994d>.
- 433 [4] Y. Deng, D. Yu, X. Cao, L. Liu, C. Rong, T. Lu, S. Liu, Structure, aromaticity and reactivity of  
434 corannulene and its analogues: a conceptual density functional theory and density functional  
435 reactivity theory study, *Mol. Phys.* 116 (2018) 956–968.  
436 <https://doi.org/10.1080/00268976.2017.1403657>.
- 437 [5] D.M. Hudgins, S.A. Sandford, Infrared Spectroscopy of Matrix Isolated Polycyclic Aromatic  
438 Hydrocarbons. 2. PAHs Containing Five or More Rings, *J. Phys. Chem. A.* 102 (1998) 344–352.  
439 <https://doi.org/10.1021/jp983482y>.
- 440 [6] D.M. Hudgins, S.A. Sandford, Infrared Spectroscopy of Matrix Isolated Polycyclic Aromatic  
441 Hydrocarbons. 1. PAHs Containing Two to Four Rings, *J. Phys. Chem. A.* 102 (1998) 329–343.  
442 <https://doi.org/10.1021/jp9834816>.
- 443 [7] D.M. Hudgins, C.W. Bauschlicher, L.J. Allamandola, Closed-shell polycyclic aromatic hydrocarbon

- 444 cations: a new category of interstellar polycyclic aromatic hydrocarbons, *Spectrochim. Acta Part A*  
 445 *Mol. Biomol. Spectrosc.* 57 (2001) 907–930. [https://doi.org/10.1016/S1386-1425\(00\)00453-4](https://doi.org/10.1016/S1386-1425(00)00453-4).
- 446 [8] S.H. Cuyllé, L.J. Allamandola, H. Linnartz, Photochemistry of PAHs in cosmic water ice, *Astron.*  
 447 *Astrophys.* 562 (2014) A22. <https://doi.org/10.1051/0004-6361/201322495>.
- 448 [9] M. Bahou, Y.-J. Wu, Y.-P. Lee, Infrared Spectra of Protonated Coronene and Its Neutral  
 449 Counterpart in Solid Parahydrogen: Implications for Unidentified Interstellar Infrared Emission  
 450 Bands, *Angew. Chemie Int. Ed.* 53 (2014) 1021–1024. <https://doi.org/10.1002/anie.201308971>.
- 451 [10] G. Rouillé, C. Jäger, M. Steglich, F. Huisken, T. Henning, G. Theumer, I. Bauer, H.-J. Knölker, IR,  
 452 Raman, and UV/Vis Spectra of Corannulene for Use in Possible Interstellar Identification,  
 453 *ChemPhysChem.* 9 (2008) 2085–2091. <https://doi.org/10.1002/cphc.200800387>.
- 454 [11] A.K. Haritash, C.P. Kaushik, Biodegradation aspects of Polycyclic Aromatic Hydrocarbons (PAHs):  
 455 A review, *J. Hazard. Mater.* 169 (2009) 1–15. <https://doi.org/10.1016/j.jhazmat.2009.03.137>.
- 456 [12] C.D. Schmidt, N. Lang, N. Jux, A. Hirsch, A Facile Route to Water- Soluble Coronenes and Benzo[  
 457 ghi ]perylenes, *Chem. – A Eur. J.* 17 (2011) 5289–5299. <https://doi.org/10.1002/chem.201003232>.
- 458 [13] T. Bauert, L. Zoppi, G. Koller, J.S. Siegel, K.K. Baldrige, K.-H. Ernst, Quadruple Anionic  
 459 Buckybowls by Solid-State Chemistry of Corannulene and Cesium, *J. Am. Chem. Soc.* 135 (2013)  
 460 12857–12860. <https://doi.org/10.1021/ja4063103>.
- 461 [14] M. Yamada, S. Tashiro, R. Miyake, M. Shionoya, A cyclopalladated complex of corannulene with a  
 462 pyridine pendant and its columnar self-assembly, *Dalt. Trans.* 42 (2013) 3300.  
 463 <https://doi.org/10.1039/c2dt32883f>.
- 464 [15] J.-L. Brédas, D. Beljonne, V. Coropceanu, J. Cornil, Charge-Transfer and Energy-Transfer  
 465 Processes in  $\pi$ -Conjugated Oligomers and Polymers: A Molecular Picture, *Chem. Rev.* 104 (2004)  
 466 4971–5004. <https://doi.org/10.1021/cr040084k>.
- 467 [16] X. Feng, W. Pisula, K. Müllen, Large polycyclic aromatic hydrocarbons: Synthesis and discotic  
 468 organization, *Pure Appl. Chem.* 81 (2009) 2203–2224. <https://doi.org/10.1351/PAC-CON-09-07-07>.
- 469 [17] K. Müllen, Evolution of Graphene Molecules: Structural and Functional Complexity as Driving  
 470 Forces behind Nanoscience, *ACS Nano.* 8 (2014) 6531–6541. <https://doi.org/10.1021/nn503283d>.
- 471 [18] Y. Yamamoto, T. Fukushima, Y. Suna, N. Ishii, A. Saeki, S. Seki, S. Tagawa, M. Taniguchi, T.  
 472 Kawai, T. Aida, Photoconductive Coaxial Nanotubes of Molecularly Connected Electron Donor and  
 473 Acceptor Layers, *Science (80-. )*. 314 (2006) 1761–1764. <https://doi.org/10.1126/science.1134441>.
- 474 [19] A.K. Geim, Random Walk to Graphene (Nobel Lecture), *Angew. Chemie Int. Ed.* 50 (2011) 6966–  
 475 6985. <https://doi.org/10.1002/anie.201101174>.
- 476 [20] A. Barbon, EPR spectroscopy in the study of 2D graphene-based nanomaterials and nanographites,  
 477 in: V. Chechik, D.M. Murphy (Eds.), *Spec. Period. Reports Electron Paramagn. Reson.*, Royal  
 478 Society of Chemistry, 2018: pp. 38–65. <https://doi.org/10.1039/9781788013888-00038>.
- 479 [21] A. Narita, X.-Y. Wang, X. Feng, K. Müllen, New advances in nanographene chemistry, *Chem. Soc.*  
 480 *Rev.* 44 (2015) 6616–6643. <https://doi.org/10.1039/C5CS00183H>.
- 481 [22] W. Yang, G. Longhi, S. Abbate, A. Lucotti, M. Tommasini, C. Villani, V.J. Catalano, A.O. Lykhin,  
 482 S.A. Varganov, W.A. Chalifoux, Chiral Peropyrene: Synthesis, Structure, and Properties, *J. Am.*  
 483 *Chem. Soc.* 139 (2017) 13102–13109. <https://doi.org/10.1021/jacs.7b06848>.
- 484 [23] N. Kheirabadi, A. Shafiekhani, The ground state of graphene and graphene disordered by vacancies,  
 485 *Phys. E Low-Dimensional Syst. Nanostructures.* 47 (2013) 309–315.  
 486 <https://doi.org/10.1016/j.physe.2012.09.022>.
- 487 [24] V. Tozzini, V. Pellegrini, Electronic structure and Peierls instability in graphene nanoribbons  
 488 sculpted in graphane, *Phys. Rev. B.* 81 (2010) 113404.  
 489 <https://doi.org/10.1103/PhysRevB.81.113404>.
- 490 [25] A. Santana, A.M. Popov, E. Bichoutskaia, Stability and dynamics of vacancy in graphene flakes:  
 491 Edge effects, *Chem. Phys. Lett.* 557 (2013) 80–87. <https://doi.org/10.1016/j.cplett.2012.11.077>.
- 492 [26] L. Andjelković, M. Gruden-Pavlović, M. Zlatar, Density functional theory study of the multimode  
 493 Jahn–Teller problem in the open-shell corannulenes and coronenes, *Chem. Phys.* 460 (2015) 64–74.  
 494 <https://doi.org/10.1016/j.chemphys.2015.05.007>.
- 495 [27] M. Tommasini, C. Castiglioni, G. Zerbi, Raman scattering of molecular graphenes, *Phys. Chem.*  
 496 *Chem. Phys.* 11 (2009) 10185. <https://doi.org/10.1039/b913660f>.

- 497 [28] F. Tampieri, A. Barbon, Resolution of EPR Signals in Graphene-based Materials from Few Layers  
 498 to Nanographites, in: D. Savchenko, A.H. Kassiba (Eds.), *Front. Magn. Reson. Electron Paramagn.*  
 499 *Reson. Mod. Carbon-Based Nanomater.*, Bentham Science, 2018: pp. 36–66.  
 500 <https://doi.org/10.2174/9781681086934118010005>.
- 501 [29] F. Tampieri, S. Silvestrini, R. Riccò, M. Maggini, A. Barbon, A comparative electron paramagnetic  
 502 resonance study of expanded graphites and graphene, *J. Mater. Chem. C* 2 (2014) 8105–8112.  
 503 <https://doi.org/10.1039/C4TC01383B>.
- 504 [30] A. Barbon, F. Tampieri, Identification of slow relaxing spin components by pulse EPR techniques in  
 505 graphene-related materials, *AIMS Mater. Sci.* 4 (2017) 147–157.  
 506 <https://doi.org/10.3934/materci.2017.1.147>.
- 507 [31] C.N.R. Rao, A.K. Sood, eds., *Graphene: Synthesis, Properties, and Phenomena*, Wiley-VCH Verlag  
 508 GmbH & Co. KGaA, Weinheim, Germany, 2013. <https://doi.org/10.1002/9783527651122>.
- 509 [32] M. Tommasini, C. Castiglioni, G. Zerbi, A. Barbon, M. Brustolon, A joint Raman and EPR  
 510 spectroscopic study on ball-milled nanographites, *Chem. Phys. Lett.* 516 (2011) 220–224.  
 511 <https://doi.org/10.1016/j.cplett.2011.09.094>.
- 512 [33] A. Barbon, M. Brustolon, An EPR Study on Nanographites, *Appl. Magn. Reson.* 42 (2012) 197–  
 513 210. <https://doi.org/10.1007/s00723-011-0285-6>.
- 514 [34] V.L.J. Joly, K. Takahara, K. Takai, K. Sugihara, T. Enoki, M. Koshino, H. Tanaka, Effect of  
 515 electron localization on the edge-state spins in a disordered network of nanographene sheets, *Phys.*  
 516 *Rev. B* 81 (2010) 115408. <https://doi.org/10.1103/PhysRevB.81.115408>.
- 517 [35] Ł. Majchrzycki, M.A. Augustyniak-Jabłokow, R. Strzelczyk, M. Maćkowiak, Magnetic Centres in  
 518 Functionalized Graphene, *Acta Phys. Pol. A* 127 (2015) 540–542.  
 519 <https://doi.org/10.12693/APhysPolA.127.540>.
- 520 [36] T.L. Makarova, A.L. Shelankov, A.I. Shames, A.A. Zyrianova, A.A. Komlev, G.N. Chekhova, D.  
 521 V. Pinakov, L.G. Bulusheva, A. V. Okotrub, E. Lähderanta, Tabby graphene: Dimensional magnetic  
 522 crossover in fluorinated graphite, *Sci. Rep.* 7 (2017) 16544. [https://doi.org/10.1038/s41598-017-](https://doi.org/10.1038/s41598-017-16321-5)  
 523 [16321-5](https://doi.org/10.1038/s41598-017-16321-5).
- 524 [37] R.E. Moss, A.J. Perry, g -factor deviations in degenerate aromatic hydrocarbon radicals: the benzene  
 525 anion, *Mol. Phys.* 22 (1971) 789–798. <https://doi.org/10.1080/00268977100103111>.
- 526 [38] T. Kato, K. Yoshizawa, T. Yamabe, Jahn–Teller effects in the coronene anions and cations, *J. Chem.*  
 527 *Phys.* 110 (1999) 249–255. <https://doi.org/10.1063/1.478100>.
- 528 [39] T. Yamabe, K. Yahara, T. Kato, K. Yoshizawa, Vibronic Coupling and Jahn–Teller Effects in  
 529 Negatively Charged Corannulene, *J. Phys. Chem. A* 104 (2000) 589–595.  
 530 <https://doi.org/10.1021/jp992496g>.
- 531 [40] H.A. Galué, C.A. Rice, J.D. Steill, J. Oomens, Infrared spectroscopy of ionized corannulene in the  
 532 gas phase, *J. Chem. Phys.* 134 (2011) 054310. <https://doi.org/10.1063/1.3540661>.
- 533 [41] A.S. Filatov, N.J. Sumner, S.N. Spisak, A. V. Zabula, A.Y. Rogachev, M.A. Petrukhina, Jahn-Teller  
 534 Effect in Circulenes: X-ray Diffraction Study of Coronene and Corannulene Radical Anions, *Chem.*  
 535 *- A Eur. J.* 18 (2012) 15753–15760. <https://doi.org/10.1002/chem.201202026>.
- 536 [42] G. Marsaglia, Choosing a Point from the Surface of a Sphere, *Ann. Math. Stat.* 43 (1972) 645–646.  
 537 <https://doi.org/10.1214/aoms/1177692644>.
- 538 [43] F. Jensen, *Introduction to Computational Chemistry*, 3rd ed., John Wiley & Sons, 2016.
- 539 [44] F. Neese, The ORCA program system, *WIREs Comput. Mol. Sci.* 2 (2012) 73–78.  
 540 <https://doi.org/10.1002/wcms.81>.
- 541 [45] G.L. Stoychev, A.A. Auer, R. Izsák, F. Neese, Self-Consistent Field Calculation of Nuclear  
 542 Magnetic Resonance Chemical Shielding Constants Using Gauge-Including Atomic Orbitals and  
 543 Approximate Two-Electron Integrals, *J. Chem. Theory Comput.* 14 (2018) 619–637.  
 544 <https://doi.org/10.1021/acs.jctc.7b01006>.
- 545 [46] E. Fawcett, J. Trotter, The crystal and molecular structure of coronene, *Proc. R. Soc. London. Ser.*  
 546 *A. Math. Phys. Sci.* 289 (1966) 366–376. <https://doi.org/10.1098/rspa.1966.0017>.
- 547 [47] S.R. Langhoff, Theoretical Infrared Spectra for Polycyclic Aromatic Hydrocarbon Neutrals, Cations,  
 548 and Anions, *J. Phys. Chem.* 100 (1996) 2819–2841. <https://doi.org/10.1021/jp952074g>.
- 549 [48] J. Oomens, B.G. Sartakov, A.G.G.M. Tielens, G. Meijer, G. von Helden, Gas-Phase Infrared

- 550 Spectrum of the Coronene Cation, *Astrophys. J.* 560 (2001) L99–L103.  
 551 <https://doi.org/10.1086/324170>.
- 552 [49] L.J. Allamandola, G.G.M. Tielens, J.R. Barker, Interstellar polycyclic aromatic hydrocarbons - The  
 553 infrared emission bands, the excitation/emission mechanism, and the astrophysical implications,  
 554 *Astrophys. J. Suppl. Ser.* 71 (1989) 733. <https://doi.org/10.1086/191396>.
- 555 [50] D.M. Hudgins, L.J. Allamandola, Infrared Spectroscopy of Matrix-Isolated Polycyclic Aromatic  
 556 Hydrocarbon Cations. 2. The Members of the Thermodynamically Most Favorable Series through  
 557 Coronene, *J. Phys. Chem.* 99 (1995) 3033–3046. <https://doi.org/10.1021/j100010a011>.
- 558 [51] M. Moreno, M.T. Barriuso, J.A. Aramburu, P. García-Fernández, J.M. García-Lastra, **Microscopic  
 559 insight into properties and electronic instabilities of impurities in cubic and lower symmetry  
 560 insulators: the influence of pressure**, *J. Phys. Condens. Matter.* 18 (2006) R315–R360.  
 561 <https://doi.org/10.1088/0953-8984/18/17/R01>.
- 562 [52] H. van Willigen, E. de Boer, J.T. Cooper, W.F. Forbes, ESR Study of the Dimer Cation of  
 563 Coronene, *J. Chem. Phys.* 49 (1968) 1190–1192. <https://doi.org/10.1063/1.1670208>.
- 564 [53] K. Komaguchi, K. Nomura, M. Shiotani, A. Lund, M. Jansson, S. Lunell, ESR and theoretical  
 565 studies of trimer radical cations of coronene, *Spectrochim. Acta Part A Mol. Biomol. Spectrosc.* 63  
 566 (2006) 76–84. <https://doi.org/10.1016/j.saa.2005.04.039>.
- 567 [54] P.J. Krusic, E. Wasserman, Coronene dication: a thermally accessible triplet, *J. Am. Chem. Soc.* 113  
 568 (1991) 2322–2323. <https://doi.org/10.1021/ja00006a072>.
- 569 [55] M.S. Blois, H.W. Brown, J.E. Marling, No Title, in: M.S. Blois (Ed.), *Symp. Free Radicals Biol.*  
 570 *Syst.*, Academic Press, New York, NY, 1961: p. 117.
- 571 [56] B.G. Segal, M. Kaplan, G.K. Fraenkel, Measurement of g Values in the Electron Spin Resonance  
 572 Spectra of Free Radicals, *J. Chem. Phys.* 43 (1965) 4191–4200. <https://doi.org/10.1063/1.1696676>.
- 573 [57] M. Sato, K. Yamamoto, H. Sonobe, K. Yano, H. Matsubara, H. Fujita, T. Sugimoto, K. Yamamoto,  
 574 Convenient synthesis and reduction properties of [7]circulene, *J. Chem. Soc. Perkin Trans. 2.* (1998)  
 575 1909–1914. <https://doi.org/10.1039/a803306d>.
- 576 [58] R.J. Angelici, B. Zhu, S. Fedi, F. Laschi, P. Zanello, Electrochemical and EPR Studies of the  
 577 Corannulene Ruthenium(II) Sandwich Complex  $[(\eta^6\text{-C}_6\text{Me}_6)\text{Ru}(\eta^6\text{-C}_{20}\text{H}_{10})](\text{SbF}_6)_2$ , *Inorg.*  
 578 *Chem.* 46 (2007) 10901–10906. <https://doi.org/10.1021/ic7015512>.
- 579 [59] M. Baumgarten, L. Gherghel, M. Wagner, A. Weitz, M. Rabinovitz, P.-C. Cheng, L.T. Scott,  
 580 Corannulene Reduction: Spectroscopic Detection of All Anionic Oxidation States, *J. Am. Chem.*  
 581 *Soc.* 117 (1995) 6254–6257. <https://doi.org/10.1021/ja00128a012>.
- 582 [60] G. Zilber, V. Rozenshtein, P.-C. Cheng, L.T. Scott, M. Rabinovitz, H. Levanon, Electron Spin  
 583 Dynamics of Photoexcited Corannulene-Lithium Complexes in Tetrahydrofuran. Fourier Transform  
 584 Electron Paramagnetic Resonance, *J. Am. Chem. Soc.* 117 (1995) 10720–10725.  
 585 <https://doi.org/10.1021/ja00148a014>.
- 586 [61] J. Janata, J. Gendell, C.-Y. Ling, W.E. Barth, L. Backes, H.B. Mark, R.G. Lawton, Concerning the  
 587 anion and cation radicals of corannulene, *J. Am. Chem. Soc.* 89 (1967) 3056–3058.  
 588 <https://doi.org/10.1021/ja00988a050>.
- 589 [62] A.J. Stone, g tensors of aromatic hydrocarbons, *Mol. Phys.* 7 (1964) 311–316.  
 590 <https://doi.org/10.1080/00268976300101081>.
- 591 [63] P.W. Atkins, A.M. Jamieson, Perturbation corrections to the g tensor, *Mol. Phys.* 14 (1968) 425–  
 592 431. <https://doi.org/10.1080/00268976800100531>.
- 593 [64] A. Zoleo, A.L. Maniero, M. Bellinazzi, M. Prato, T. Da Ros, L.C. Brunel, M. Brustolon, Radical  
 594 anions of fullerene bisadducts: a multifrequency CW-EPR study, *J. Magn. Reson.* 159 (2002) 226–  
 595 236. [https://doi.org/10.1016/S1090-7807\(02\)00032-0](https://doi.org/10.1016/S1090-7807(02)00032-0).
- 596 [65] M.G. Townsend, S.I. Weissman, Possible Symptom of the Jahn- Teller Effect in the Negative Ions  
 597 of Coronene and Triphenylene, *J. Chem. Phys.* 32 (1960) 309–310.  
 598 <https://doi.org/10.1063/1.1700934>.
- 599 [66] H.M. McConnell, A.D. McLachlan, Nuclear Hyperfine Interactions in Orbitally Degenerate States  
 600 of Aromatic Ions, *J. Chem. Phys.* 34 (1961) 1–12. <https://doi.org/10.1063/1.1731545>.
- 601 [67] I.C. Lewis, L.S. Singer, Electron Spin Resonance of Radical Cations Produced by the Oxidation of  
 602 Aromatic Hydrocarbons with  $\text{SbCl}_5$ , *J. Chem. Phys.* 43 (1965) 2712–2727.

603 <https://doi.org/10.1063/1.1697200>.  
604 [68] T. Sato, H. Tanaka, A. Yamamoto, Y. Kuzumoto, K. Tokunaga, Jahn–Teller effect in coronene  
605 monoanion: A comparative study with corannulene monoanion, *Chem. Phys.* 287 (2003) 91–102.  
606 [https://doi.org/10.1016/S0301-0104\(02\)00981-3](https://doi.org/10.1016/S0301-0104(02)00981-3).  
607 [69] T. Sato, A. Yamamoto, H. Tanaka, An ESR study on Jahn–Teller effect in corannulene monoanion,  
608 *Chem. Phys. Lett.* 326 (2000) 573–579. [https://doi.org/10.1016/S0009-2614\(00\)00759-4](https://doi.org/10.1016/S0009-2614(00)00759-4).  
609 [70] T. Sato, A. Yamamoto, T. Yamabe, Electronic and Vibrational Structures of Corannulene Anions, *J.*  
610 *Phys. Chem. A.* 104 (2000) 130–137. <https://doi.org/10.1021/jp992912x>.  
611 [71] J.R. Bolton, A. Carrington, The effects of orbital degeneracy in the E.S.R. spectrum of the coronene  
612 positive ion, *Mol. Phys.* 4 (1961) 271–272. <https://doi.org/10.1080/00268976100100401>.  
613